PAPER

Destabilization of counter-propagating Alfvénic instabilities by tangential, co-current neutral beam injection

To cite this article: M. Podestà *et al* 2018 *Nucl. Fusion* **58** 082023

IOP Publishing | International Atomic Energy Agency Nuclear Fusion

Nucl. Fusion **58** (2018) 082023 (11pp) https://doi.org/10.1088/1741-4326/aab4ae

Destabilization of counter-propagating Alfvénic instabilities by tangential, co-current neutral beam injection

M. Podestà, E.D. Fredrickson and M. Gorelenkova

Princeton Plasma Physics Laboratory, Princeton NJ 08543, United States of America

E-mail: mpodesta@pppl.gov

Received 4 December 2017, revised 14 February 2018
Accepted for publication 7 March 2018
Published 29 June 2018

Abstract

Injection of high-energy neutrals is a common tool to heat the plasma and drive current non-inductively in fusion devices. Once neutrals ionize, the resulting energetic particles can drive instabilities that are detrimental for the performance and the predictability of plasma discharges. A broad deposition profile of neutrals from neutral beam injection, e.g. by aiming the beam tangentially on the outboard midplane (i.e. off-axis), is often assumed to limit those undesired effects by reducing the radial gradient of the EP density, thus reducing the drive for instabilities. However, this work presents new evidence that tangential neutral beam injection, including off-axis injection near the plasma mid-radius, can also lead to undesired effects such as the *destabilization* of Alfvénic instabilities. Time-dependent analysis with the TRANSP code indicates that instabilities are driven by a combination of radial and energy gradients in the distribution function of the energetic particles. The mechanisms for wave-particle interaction revealed by the energetic particle phase space resolved analysis are the basis to identify strategies to mitigate or suppress the observed instabilities.

Keywords: Alfvénic instabilities, spherical tokamak, NSTX-U, neutral beam injection, counter-propagating TAEs

(Some figures may appear in colour only in the online journal)

1. Introduction

The reliable operation of fusion reactors such as ITER requires accurate predictions of scenarios that feature large populations of energetic particles (EP) from fusion reactions, neutral beam injection (NBI) and rf waves. Although NBI is a well-proven tool for heating and current drive, the resulting EP population can drive instabilities such as Alfvénic modes [1–5] that typically cause a degradation in performance. If significant EP losses are induced, damage of vacuum vessel components can also occur.

The NBI geometry affects the radial profile of the resulting EP population. For example, NB injection that is aimed at or inside the magnetic axis of a fusion device typically results in peaked EP profiles. Conversely, aiming the NB injection in between the axis and the plasma periphery (known as *off-axis NBI*) tends to broaden the EP profile. In particular, scenarios with a broad EP pressure profile from off-axis NBI are usually thought to be effective in limiting EP-driven modes, under the main assumption that the drive from the radial EP density gradient is the main energy source for the instabilities. Examples from recent experiments are reported, for example, in [6].

This work presents two main results on destabilization of instabilities by NB injection. First, in contrast with previous observations, this work reports the first experimental evidence of the *destabilization* of toroidicity-induced Alfvén Eigenmodes (TAEs) by off-axis, co-current NBI with the observed TAEs propagating in the *counter*-current direction in spite of the co-NB injection. In some cases, experimental observations can be qualitatively explained by inversions in the radial gradient of the EP density. However, in general, the intrinsic coupling between EP redistribution in energy and radius (caused by wave-particle interactions) must be considered for a more quantitative understanding of the experimental

results. This is confirmed by discharges for which counter-propagating modes are detected although no inversion in the NB ion density is observed.

The experimental results suggest that the formation of EP distributions with inverted fast ion energy gradients caused by simultaneous NB and rf injection in reactors such as ITER can further reduce the stability of counter-propagating TAEs [7, 8]. Therefore, reliable predictions for future scenarios on ITER and other reactor-grade devices (including reactors based on the stellarator concept) should be based on analyses that include the entire EP phase space dynamics, especially when a complex EP distribution function is expected from the synergy between fusion reactions, NBI and rf heating. The second main result of this work is that phase space effects can be properly taken into account to provide quantitative results in the framework of integrated tokamak simulations, in which the evolution of both thermal plasma and EPs is solved consistently.

In the remainder of the paper, the experimental scenarios under investigation are first illustrated in section 2. The methodology for mode stability analysis is introduced in section 3, followed by the results on linear stability (section 3.1) and by a discussion of the mode saturation mechanisms (section 3.2). The main findings of this work are summarized in section 4.

2. Experimental scenarios

This work is based on experimental observations from the commissioning campaign of the National Spherical Torus Experiment Upgrade device (NSTX-U [9]), which is equipped with up to 12 MW of neutral beam power for non-inductive heating and current drive. NSTX-U is a small aspect ratio device (major/minor radius are 0.95 m and 0.65 m respectively) operating at nominal magnetic field $B_T \leqslant 1$ T and plasma current $\leqslant$2 MA. The experiments discussed herein are low-confinement mode, deuterium plasmas with $B_0 = 0.65$ T toroidal field on axis. Central density and temperature are $n_e \approx 2{-}4 \times 10^{19}$ m^{-3} and $T_e \leqslant 1$ keV (subscripts e, i refer to electrons and ions, respectively). Note that, since no measurements of ion temperature and velocity are available from the NSTX-U charge-exchange recombination diagnostic when the tangential sources are firing, it is assumed that ion and electron temperatures are approximately equal. Also, toroidal velocity is assumed to be zero, which is clearly unrealistic but simplifies the analysis in the absence of reliable measurements.

Representative plasma parameters are shown in figure 1. With only 0.9–1 MW of injected NB power at injection voltage 60–65 kV from a single NB source, plasmas remain in L-mode. The safety factor profile evolves in time, with central value q_0 approaching 1 and edge values typically 5–10 based on the plasma current. Plasma current increases during the time of interest, $100 \leqslant t \leqslant 400$ ms, and reaches 0.9 MA during flat-top (figure 1(b)). A common feature for NSTX-U discharges exhibiting counter-propagating TAEs is NB injection of $\approx$1 MW in the co-current direction from a NB source aimed at a tangency radius larger on the low-field-side with respect to the magnetic axis ($R_{\rm tan} = 130$ cm for the discharge in figure 1, that is near mid-radius on the outboard midplane). For the measured thermal plasma parameters, NB ions are super-Alfvénic with $v_{\rm fast}/v_{\rm Alfven} \approx 1$ at early times and $v_{\rm fast}/v_{\rm Alfven} \gtrsim 2$ as the density increases (where $v_{\rm fast}$ is the fast ion velocity corresponding to the injection energy and $v_{\rm Alfven}$ is the central Alfvén velocity).

Soon after NB injection starts, TAEs are driven unstable by the increasing population of fast particles. Figure 1(a) shows the mode number spectrum of magnetic fluctuations measured at the plasma edge by Mirnov coils, from which toroidal mode numbers $|n| = 1, 2$ are computed. The direction of propagation of the TAEs is inferred from the relative phase of detectors distributed toroidally around the vacuum vessel. Early in time, TAEs propagate in the co-NB injection direction. However, at later times a reversal in the direction of propagation is observed and TAEs propagate in the *counter*-NB injection direction after 300 ms. Figure 2(a) shows the profiles of fast ion density computed by TRANSP at different times during the discharge. (Examples of computed TAE radial mode structures are also shown and will be discussed in section 3.) One clear feature from figure 2(a) is the modification of the profile from monotonic at early times to hollow at later times.

A second experimental scenario investigated in this work is shown in figure 3 for NSTX-U discharge #205072. The NB timing and mix of NB sources are considerably different from the discharge shown in figures 1 and 2. In particular, only a tangential NB source aimed outside the magnetic axis (source 2A) is active for $t > 240$ ms. The spectrum of magnetic fluctuations is richer than in the discharge discussed previously. Dominant mode numbers are $n = 2{-}4$ for co-propagating TAEs and $|n| = 1{-}2$ for counter-propagating modes. One complication in this discharge is the presence of several modes at comparable frequency, and possibly with opposite direction of propagation. In some cases, this causes the toroidal mode number identification to fail. Nevertheless, the main features are retained as can be inferred by comparing the toroidal mode number spectrum (figure 3(a)) with the frequency spectrum of raw magnetic fluctuations (figure 3(c)).

The two discharges discussed above are representative of the conditions for which counter-propagating TAEs have been observed so far on NSTX-U. The common feature is the NB injection with off-axis sources at the low-field side. More detailed scans of parameters, e.g. to vary the NB mix of on- versus off-axis NB sources, are not available from the initial commissioning campaign of NSTX-U and are deferred to the next experimental campaign.

3. TRANSP analysis of TAE destabilization mechanisms

The destabilization of counter-TAEs is investigated through the time-dependent tokamak transport code TRANSP [10][1], whose NB module NUBEAM [11, 12] has been recently enhanced with a physics-based, reduced model for fast ion transport by instabilities (called *kick model* [13, 14]). The kick

[1] For more details on the TRANSP code, please refer to the TRANSP webpage at http://w3.pppl.gov/~pshare/help/transp.htm.

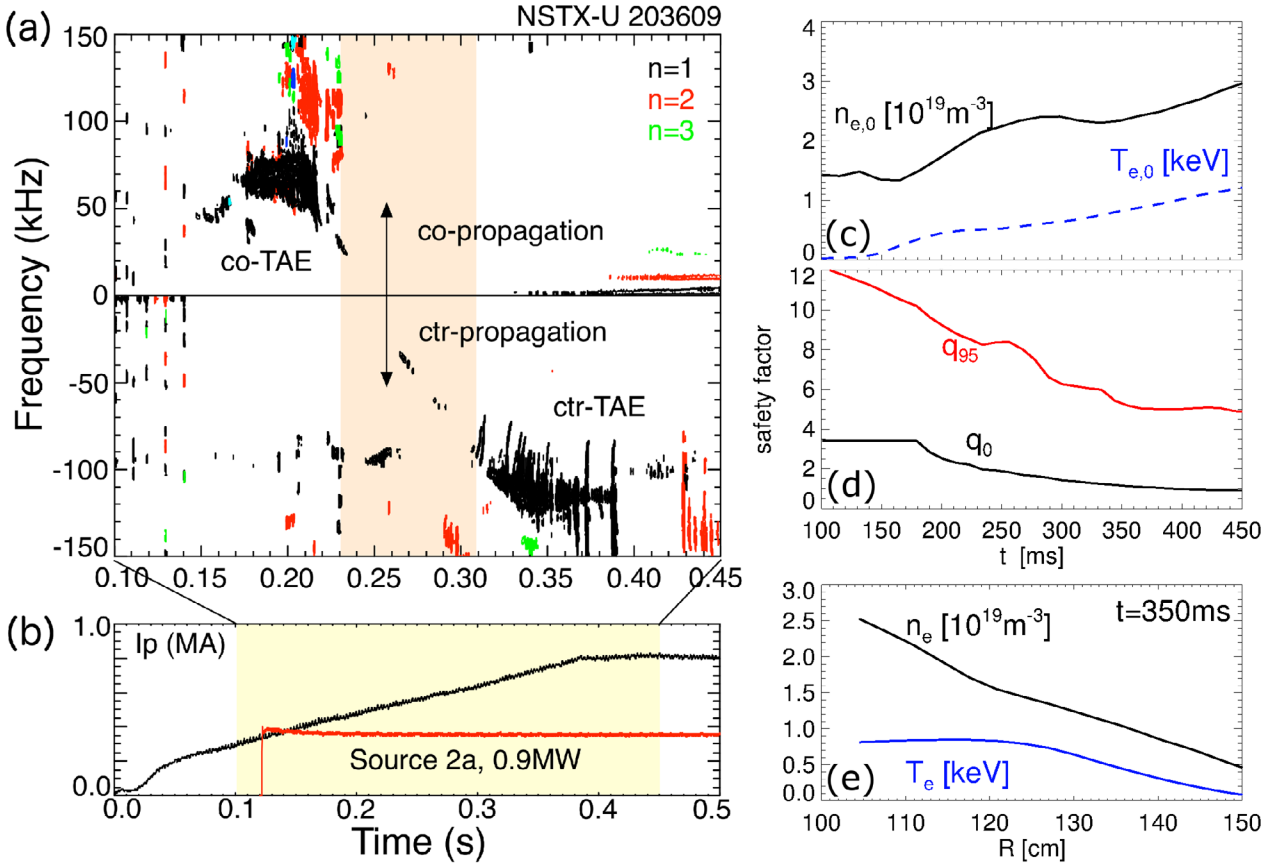

Figure 1. (*a*) Spectrum of magnetic fluctuations measured by Mirnov coils. Counter-propagating modes are here shown with negative frequency. (*b*) Waveforms of plasma current (black) and injected NB power (red). (*c*) Time evolution of central electron density and temperature. (*d*) Evolution of central and edge values of the safety factor. (*e*) Electron density and temperature profiles at $t = 350$ ms. The magnetic axis is at $R \approx 105$ cm.

model in NUBEAM/TRANSP is here used to compute mode stability (linear growth rate $\gamma_{\rm lin}$), hence the net growth rate $\gamma_{\rm net}$ that includes damping rates from the ideal magneto-hydrodynamics code NOVA and its kinetic extension NOVA-K [15–17]. Thermal plasma profiles are used as input for the NOVA code to compute the TAE eigenmodes and their radial mode structure. Because of the lack of experimental measurements of toroidal plasma rotation, the NOVA analysis assumes zero velocity, i.e. no Doppler-shift of the mode frequency and TAE continuum are accounted for. Moreover, the zero-rotation approximation implies that co- and counter-propagating eigenmodes have the same radial structure (a finite rotation would introduce an asymmetry in the TAE continuum for opposite propagation directions, possibly resulting in different structure and frequency of the eigenmodes [18]).

Since the background profiles and the fast ion distribution evolve over time for the scenarios investigated in this work, the NOVA analysis is performed at two representative times corresponding to the peak activity of TAEs for each of the two representative discharges. The NOVA analysis provides a set of candidate eigenmodes that *may* exist in the target scenario, based on their stability properties quantified through the balance of mode drive and damping. To select the unstable modes, eigenmodes from NOVA are first used in the particle following code ORBIT [19] to compute the phase-space resolved transport probability matrix associated with each mode [13]. Each matrix $p(\Delta E, \Delta P_\zeta | E, P_\zeta, \mu)$ represents the probability that a fast ion with phase space coordinates (E, P_ζ, μ) experiences *kicks* $(\Delta E, \Delta P_\zeta)$ over a fixed time interval as a result of the interaction with a mode at normalized amplitude $A = 1$. Fast ion coordinates in phase space are identified by the constants of motion E, P_ζ and μ [20]. E is the total particle energy. $P_\zeta = \rho_\parallel g/\Psi_w - \Psi_{\rm pol}$ is the canonical angular momentum ($\rho_\parallel$: parallel particle momentum; $g \sim B/R$: the g-function; $\Psi_{\rm pol}$: poloidal flux; Ψ_w: value of $\Psi_{\rm pol}$ at the wall). μ is the magnetic moment. The representation of wave-particle interaction in terms of a probability is well suited to distill information from a particle following code such as ORBIT and transfer it to the Monte Carlo module NUBEAM. Probability matrices can therefore be used in TRANSP/NUBEAM to investigate the mode's stability [14], with the kick model providing information on the energy exchange between a sample fast ion population and the mode, from which the mode's drive can be computed.

Figure 4 illustrates the advantage of adopting phase space over real space representation to investigate mode stability. Orbits are shown for two particles with same initial energy $E = 20$ keV and initial position at the mid-plane $\Psi_{\rm pol} = 0.285$ and $\Psi_{\rm pol} = 0.3$, respectively. The initial toroidal location is chosen randomly from $[0, 2\pi]$. After interacting for 4 ms with

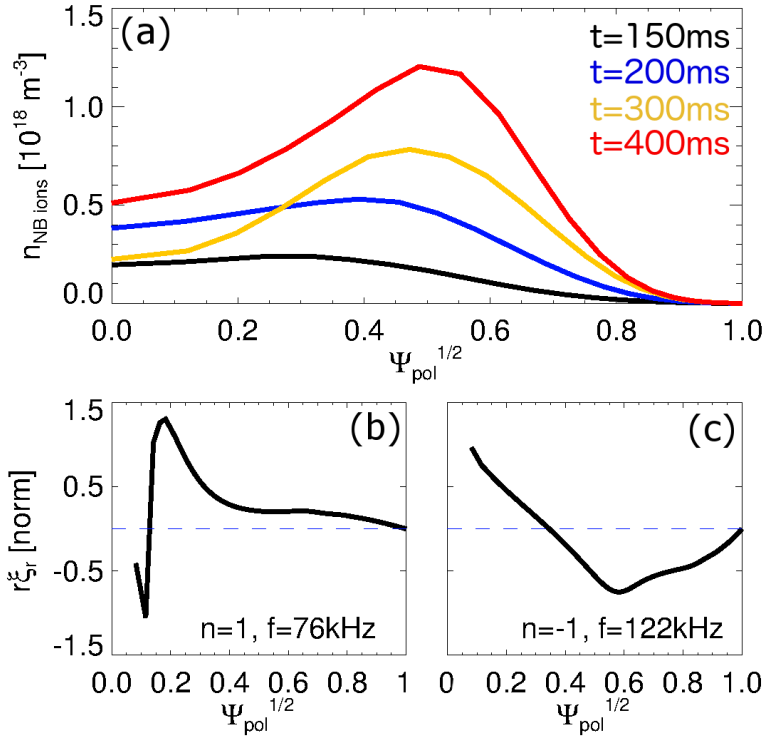

Figure 2. (*a*) NB ion density profile versus time. (*b*) and (*c*) Radial displacement, $r\xi_r$, for co- and counter-propagating $|n| = 1$ TAE eigenmodes from NOVA analysis. (r: normalized minor radius variable in NOVA).

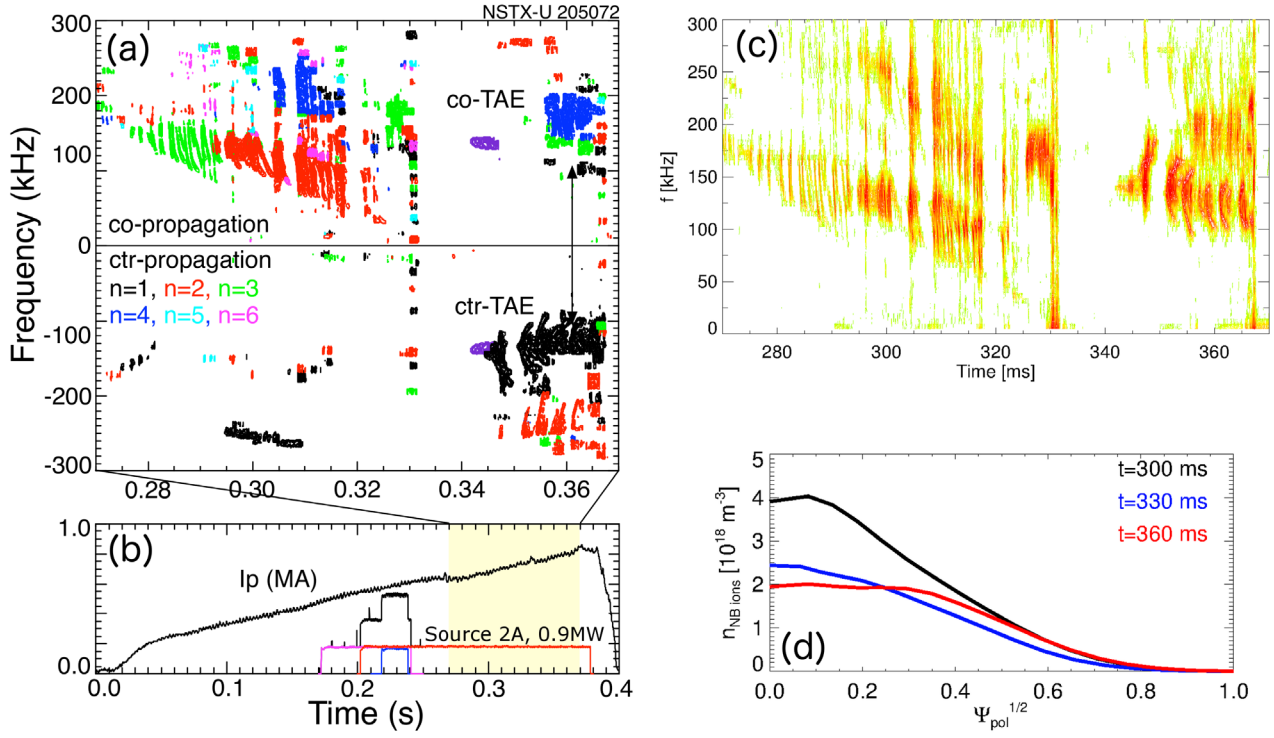

Figure 3. (*a*) Spectrum of toroidal mode numbers inferred from magnetic fluctuations measured by Mirnov coils. Counter-propagating modes are here shown with negative frequency. (*b*) Waveforms of plasma current (black) and injected NB power (red). (*c*) Raw spectrum of magnetic fluctuations showing the overlap of co- and counter-propagating modes with comparable frequency. (*d*) Fast ion density profiles at three representative times during the discharge. The magnetic axis is at $R \approx 105$ cm.

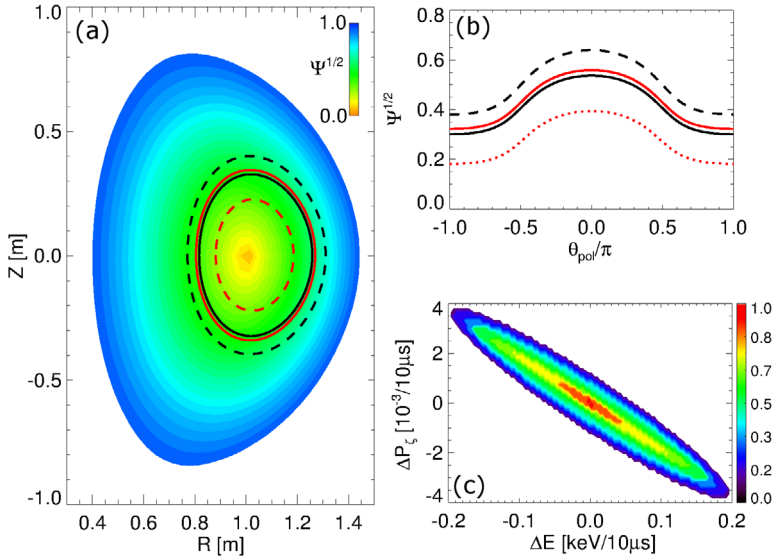

Figure 4. (*a*) Poloidal cross-section with contours at constant poloidal flux, $\Psi^{1/2}$. Lines show orbits for $E = 20\,\mathrm{keV}$ particles (solid) that gain (black, dashed) or lose (red, dashed) energy through interaction with a counter-TAE. (*b*) Particle position versus poloidal angle. Note the large departure from the initial flux surface ($\theta_{\mathrm{pol}} = 0$) during the orbiting. (*c*) Kick probability associated with the particle's (E, P_ζ, μ) for the counter-TAE of figure 2(*c*).

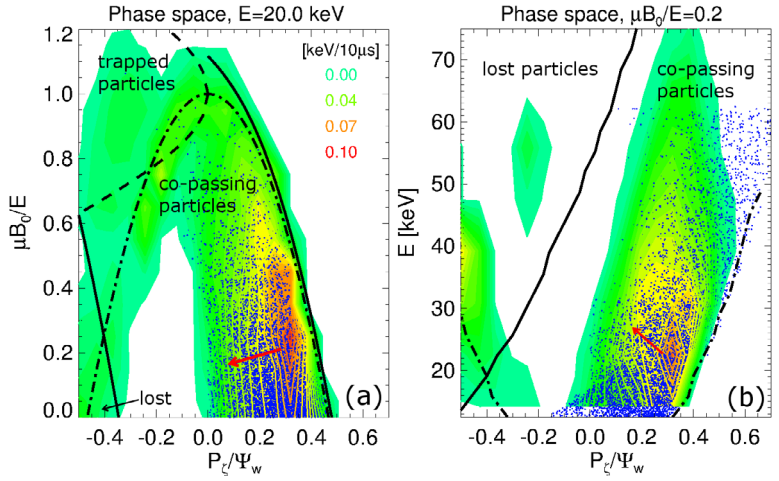

Figure 5. Contours show the phase space map of the root-mean-square energy kicks from the counter-TAE in figure 2(*c*). Lines represent boundaries between different types of orbit. Dots are a sample of the fast ion distribution from NUBEAM/TRANSP. The red arrows illustrate simple trajectories caused by the coupling between E and P_ζ variations. Since $\Delta P_\zeta/\Delta E < 0$ for the counter-propagating mode, particles that move outward (decreasing P_ζ) will tend to gain energy. (*a*) Slice of the (E, P_ζ, μ) phase space at constant energy, $E = 20\,\mathrm{keV}$. (*b*) Slice of phase space at constant $\mu B_0/E = 0.2$.

a counter-TAE (see radial mode structure in figure 2(*c*)), one particle gains energy and the other loses energy, with $|\Delta E| = 4$ keV. Away from the mid-plane, particles depart from the initial position and explore a large radial range of Ψ_{pol} even in the absence of any perturbation (figure 4(*b*)). During interaction with the mode, the particles' orbit become a complicated function of space and time. The same orbits appear as simpler trajectories in terms of (E, P_ζ, μ), with the effect of the mode represented by the kick probability shown in figure 4(*c*) (also see figure 5 below).

The correlation between energy and P_ζ changes visible in figure 4(*c*) is expected from the fundamental relationship induced by resonant wave-particle interactions, with $\Delta P_\zeta/\Delta E \sim n/\omega$ (ω: angular mode frequency) [20]. Inclusion of correlated ΔE and ΔP_ζ kicks over the phase space (E, P_ζ, μ) in TRANSP/NUBEAM is at the basis of the kick model. Kicks associated with a specific instability are represented in the Monte Carlo NUBEAM module through a *transport probability matrix*, $p(\Delta E, \Delta P_\zeta | E, P_\zeta, \mu)$, which represents the probability that a fast particle with variables (E, P_ζ, μ) receives correlated kicks $\Delta E, \Delta P_\zeta$ over a small step during its orbiting. The probability is computed through particle-following codes such as ORBIT [19] that can track the evolution of (E, P_ζ, μ) of each particle in the presence of a given instability, from which ΔE and ΔP_ζ are reconstructed. (More details can be found in the appendix of [14]).

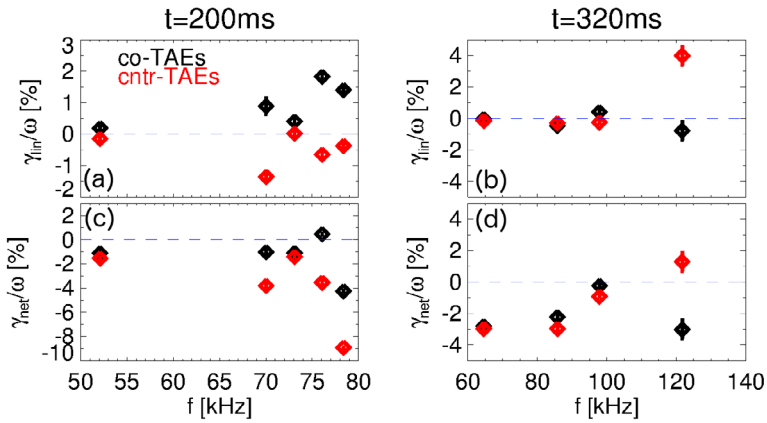

Figure 6. NSTX-U discharge #203609, see figures 1 and 2. Linear stability through TRANSP and kick model for co-TAEs (black) and counter-TAEs (red). (*a*) and (*b*) Linear growth rate. (*c*) and (*d*) Net linear growth rate, including damping rate from NOVA-K.

General features of energy and P_ζ variations associated with a specific instability can be visualized over the entire phase space by considering root-mean-square (rms) kick values as a function of (E, P_ζ, μ). The average value of the kicks can be interpreted as an indicator of the strength of wave-particle interactions in different regions of phase space, with larger kicks typically occurring when a resonance condition is satisfied. For example, figure 5 shows rms energy kicks resulting from the counter-propagating TAE mode in figure 2(*c*) for two-dimensional slices of the (E, P_ζ, μ) phase space at constant E and at constant μ, shown in panels *a* and *b* respectively. One notable feature is the large variation of the probabilities—and associated rms kicks—over the (E, P_ζ, μ) space. This results from the localization of resonances in phase space and from the (generally) large number of resonances associated with each mode. Another important feature is the relative localization of fast ion tracers (blue dots in figure 5) with respect to the resonances, which ultimately determine the absolute strength of the interaction. For instance, a complete misalignment of the fast ion distribution from the resonance location would result in essentially null interaction.

3.1. Linear stability analysis

For each discharge, kick probabilities are computed for all candidate eigenmodes from NOVA, then used in TRANSP to infer the mode stability. Within the kick model, linear stability is computed from the balance of power transferred from fast ions to each mode included in the simulation and the power lost by the mode through damping in the limit of vanishing mode amplitude [14]. Stability calculations include damping rates computed through NOVA. In the present analysis, the dominant terms are ion/electron Landau damping and continuum damping for modes that intercept the TAE continuum.

In the following, linear stability results are presented for both discharges introduced in section 2. More detailed analysis is then presented for discharge #203609, featuring a hollow EP density profile, since its fluctuation spectrum with only one dominant mode results in a more straightforward interpretation of the analysis results. (For instance, linear stability for each of the modes in #205072 may be affected by the presence of other, saturated modes possibly causing EP redistribution, thus—in turn—affecting the stability results).

For discharge #203609, only two of the original eigenmodes from NOVA are found to be unstable, namely a co-TAE with frequency $f \approx 76$ kHz at $t = 200$ ms and a counter-TAE with $f \approx 122$ kHz at $t = 320$ ms, see figure 6. Their radial mode structure is shown in figures 2(*b*) and (*c*). Only these two modes are retained in the following analysis.

More details of the linear stability results for the two unstable modes are presented in figure 7. For the co-propagating TAE, the linear growth rate exceeds the damping rate after 150 ms, it increases rapidly up to ≈180 ms and then decreases until the mode is stabilized. The counter-propagating mode shows the opposite behavior. The linear growth rate is *negative* at earlier times, then increases and the mode is destabilized after ≈250 ms. Because of the fast variation in background plasma profiles, however, the validity of the computed transport probability is questionable outside time windows of ±30 ms and ±50 ms from the selected times $t = 200$ ms and $t = 320$ ms, respectively(since profiles evolve on slower time scales at later times, the time window around 320 ms is broader than that around 200 ms). Nevertheless, the trends shown in figure 7(*a*) appear quite robust and overall consistent with the experimental behavior of the modes, see figure 1(*a*).

Figures 7(*b*) and (*c*) show the radial profiles of power transferred from fast ions to each mode in the limit of vanishing mode amplitude (*linear* phase). It can be seen that most of the power is exchanged around $\Psi_{\rm pol} = 0.2-0.5$, that is in the region of inverted radial gradient for $t \geqslant 200$ ms (figure 2(*a*)). Note that regions with both positive (destabilizing) and negative (stabilizing) energy transfer from the fast ions to the mode are observed, in spite of the monotonic density gradient. This reflects the competition between drive and damping by fast ions associated with the location of resonances in phase space, rather than in real space only.

As discussed in section 2, the AE stability results for discharge #203609 are based on the assumption that $T_e = T_i$, which introduces uncertainties in the calculation of ion Landau damping through NOVA-K. To quantify the uncertainties, figure 8(*a*) shows a comparison of the measured electron

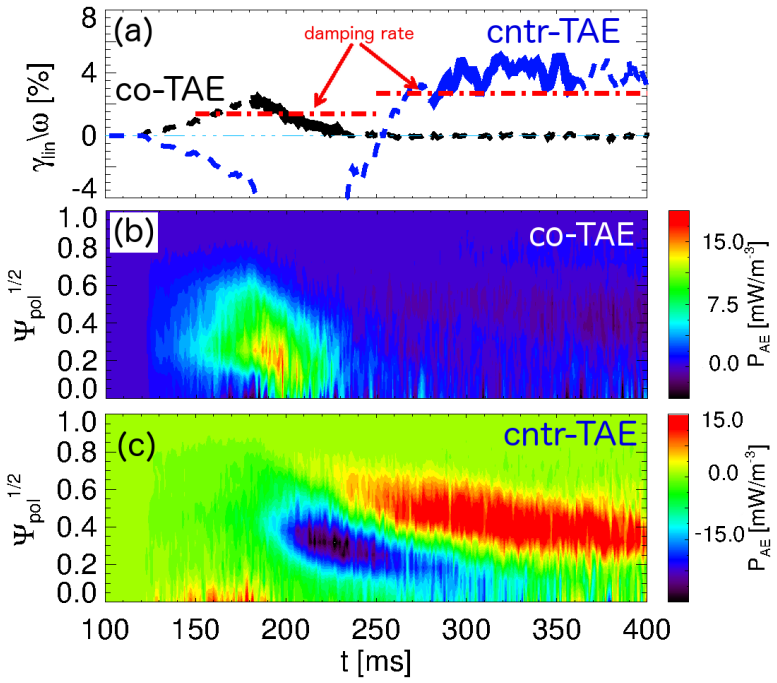

Figure 7. (*a*) Linear growth rate of the most unstable $n = 1$ TAEs versus time. Solid, thick lines are used over the time range of reliable results for $\gamma_{\rm lin}/\omega$. Dashed lines indicate the time range over which kick model results become unreliable because of the departure of plasma profiles from those at the nominal times at which transport probabilities are computed. Red dot-dashed line is the damping rate from NOVA-K. (*b*) and (*c*) Radial profile of the power exchanged between fast ions and the mode in the linear phase. Positive power means energy is transferred from the particles to the wave.

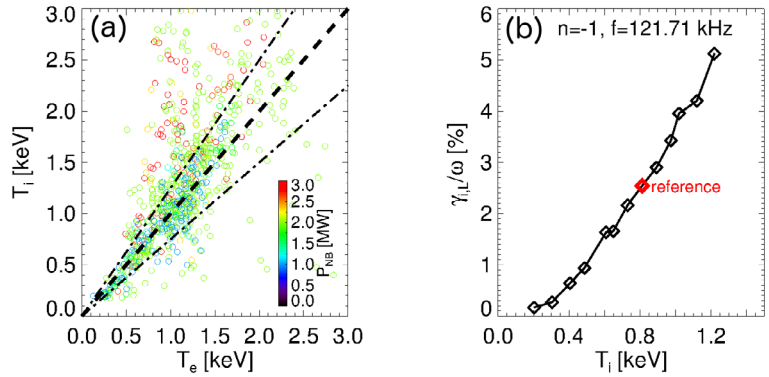

Figure 8. (*a*) Measured electron versus ion temperature at the magnetic axis from 60 NSTX discharges and 15 NSTX-U discharges. Symbols are color-coded based on the injected NB power at the time of measurements. Dashed and dot-dashed lines indicate where $T_i = T_e$ and $T_i = T_e \pm 25\%$, respectively. (*b*) Ion Landau damping from NOVA-K versus ion temperature for the $n = -1$ mode in figure 2(*c*). The T_i value used for the simulations discussed in this work is marked as *reference*.

and ion temperature for a set of NSTX and NSTX-U discharges with injected NB power up to 3 MW. At low injected power $\approx$1 MW (comparable to the level used in #203609) the maximum spread in measured central ion temperature is roughly $T_i \approx T_e \pm 25\%$, with larger discrepancies observed at higher injected NB power $\gtrsim$2 MW. The implications for the computed ion Landau damping, $\gamma_{i,L}$, are illustrated in figure 8(*b*) for the counter-TAE of figure 2(*c*). Given the strong dependence of $\gamma_{i,L} = \gamma_{i,L}(T_i)$, a $\pm$25% difference in T_i results in variations as large as $\pm$40% in the computed damping. (Similar results are obtained for the co-propagating TAE in figure 2(*b*)). In general, uncertainties in the measurements result in additional uncertainty in the predicted onset and decay times of the instabilities (see figure 7(*a*)), especially for scenarios during the plasma current ramp-up with rapidly varying parameters.

To complement the results from discharge #203609, figure 9 shows the linear stability results for discharge #205072 that is characterized by a flat or monotonic radial profile of fast ion density and tangential NB injection aimed just outside the magnetic axis (tangency radius $R_{\rm tang} = 110$ cm). At earlier times (around $t = 300$ ms) several co-propagating TAEs with $n = 1-4$ are predicted to be unstable, which is consistent with the experimental data shown in figure 3(*a*). Also consistent with the experiment is the increase in the drive for counter-propagating TAEs at later times, around $t = 360$ ms.

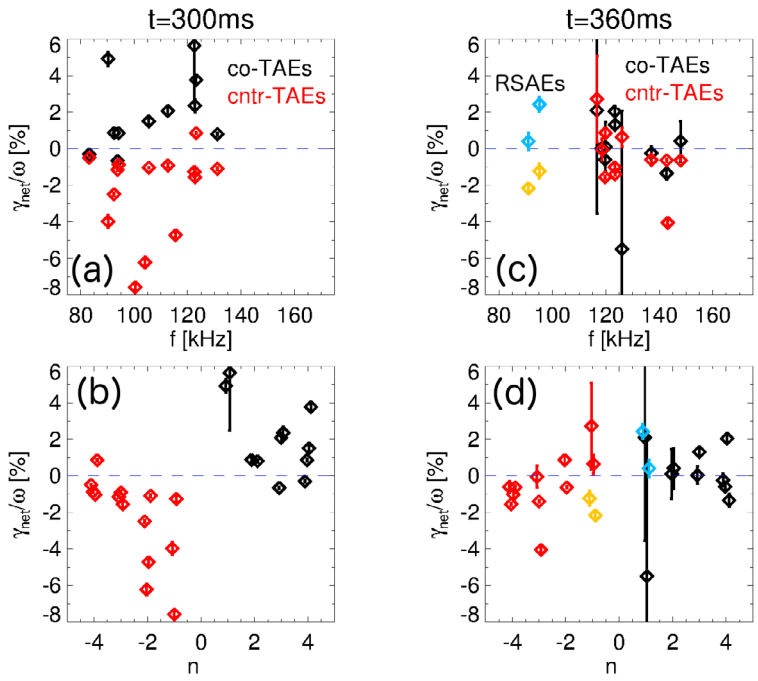

Figure 9. NSTX-U discharge #205072, see figure 3. Linear stability through TRANSP and kick model for co-TAEs (black) and counter-TAEs (red). (*a*) and (*b*) Net linear growth rate, including damping rate from NOVA-K, computed at $t = 300$ ms. Results are shown as a function of frequency (top) and mode number (bottom). (*c*) and (*d*) Net growth rates at $t = 360$ ms. Light colors are used to mark $|n| = 1$ modes identified as RSAEs. (For clarity, points are slightly shifted from their nominal toroidal mode numbers in panels (*b*) and (*d*)).

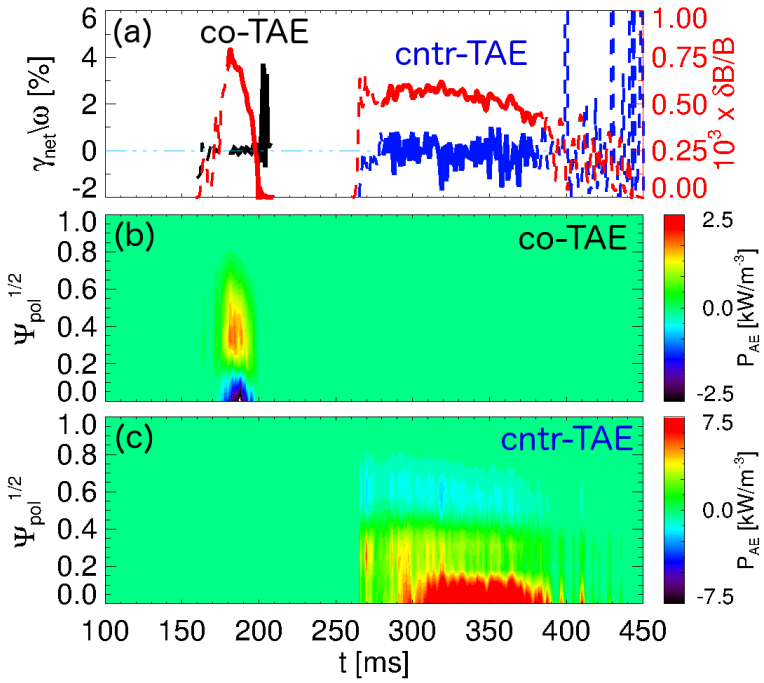

Figure 10. (*a*) Black, blue: net growth rate near saturation. Red: saturation amplitude of most unstable $|n| = 1$ TAEs. Dashed lines indicate the time range over which kick model results are unreliable. (*b*) and (*c*) Radial profile of the power exchanged between fast ions and the mode in the saturated phase.

Noticeably, for this discharge co-TAEs are not stabilized when counter-TAEs are unstable, which is in contrast with #203609 results.

It should be mentioned that some discrepancies between predicted and measured spectra are also observed. For example, simulations indicate that an $n = -4$ TAE should be unstable at $t = 300$ ms, but the mode is not observed in the experiment. Instead, there are indications of a (weakly) unstable, transient $n = -1$ mode. Also, simulations find at least two reversed-shear $|n| = 1$ AE modes (RSAEs) unstable

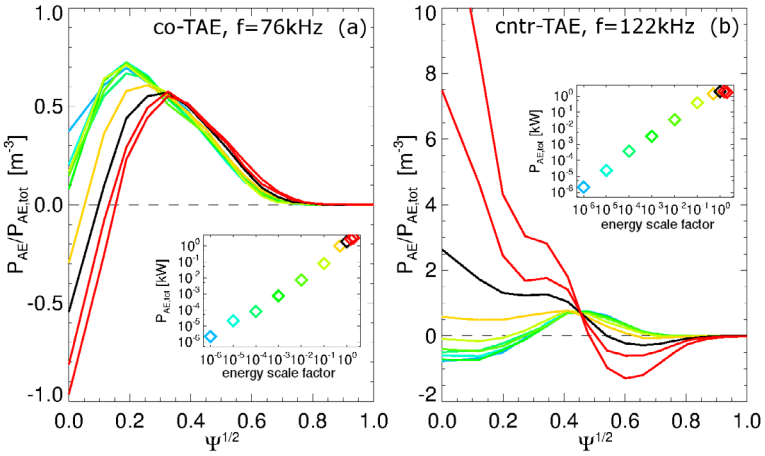

Figure 11. Radial profile of power exchange between fast ions and co/counter-TAEs as the wave energy is increased. The insets show the total power versus wave energy scaling factor, where a factor 1 corresponds to the nominal saturation amplitude. All profiles are evaluated at $t = 200$ ms and $t = 320$ ms for the co- and counter-TAE, respectively.

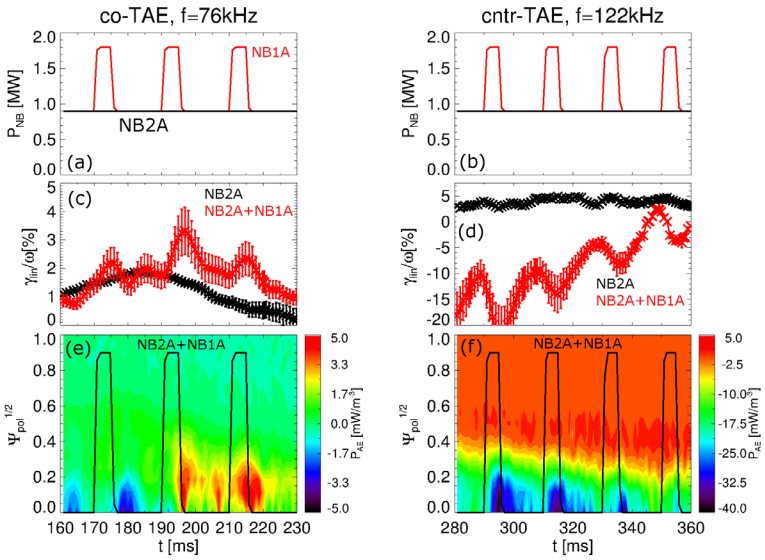

Figure 12. (*a*) and (*b*) Injected NB power from the actual source used in the experiment (NB2A) and from the additional source introduced in TRANSP (NB1A). Linear growth rates for (*c*) co- and (*d*) counter-TAE modes are shown for the NB2A-only and NB2A + NB1A cases. (*e*) and (*f*) Computed power density exchanged between TAE and fast ions as a function of time and normalized minor radius. (Positive power means energy flowing from the fast ions to the mode).

at $t = 360$ ms at frequencies below those of the unstable TAEs. These modes are not observed in the experiment, arguably because of the beta-suppression mechanism discussed in [21]. Finally, $n = 1$ modes are predicted to be the most unstable modes around $t = 300$ ms, which is not supported by the experimental evidence since only weak $n = 1$ activity is in fact measured. (Note, however, that this observation does not include information on the predicted saturation amplitudes).

The simulation results for discharge #205072 are therefore less conclusive than those for the simpler scenario from #203609. Nevertheless, the general features from the experiment are recovered, namely the transition from the usual scenario with dominant co-propagating TAEs to a scenario with enhanced drive for counter-TAEs, which can co-exist with the co-propagating modes.

3.2. Mode saturation analysis

In addition to the linear stability analysis, estimates of the expected saturation amplitudes are available for discharge #203609. As unstable modes evolve beyond the initial linear phase and grow to a finite amplitude, fast ions respond to the instabilities and the linear response (see figure 7) is modified accordingly. Saturation amplitude can be estimated through the kick model by computing the mode amplitude for which power transferred from fast ions to the modes equals the power dissipated through damping [14].

The inferred saturation amplitudes are $\delta B/B \sim 5{-}10 \times 10^{-4}$ (δB: perturbation of the magnetic field), as shown in figure 10, which is roughly consistent with previous measurements on NSTX through reflectometry [14]. By comparing linear and saturated regimes, it is clear that the wave-particle interaction

modifies the fast ion distribution, as seen for example from the modification of the power density profiles in panels (*b*), (*c*) of figures 7–10. Changes in the profile when the square of mode amplitude (proportional to the wave energy) is scaled are shown in figure 11 for two representative times. The response of the fast ions causes a significant departure at saturation with respect to the linear phase. For instance, the counter-TAE shows a reversal of the power density profile as the amplitude increases. Notably, from figure 11 the total power exchanged near and above saturation remains nearly constant, but the power density profile continues to evolve.

4. Discussion and conclusions

The competition between drive and damping by fast ions revealed by the stability analysis, along with the correlation $\Delta P_\zeta/\Delta E \sim n/\omega$, has three important implications. First, it indicates that a simple linear stability analysis may not be representative of the mode's behavior near saturation (i.e. when modes eventually become relevant in real experiments). Second, analysis based on the effect of a radial fast ion density gradient alone may lead to incomplete or erroneous predictions for the mode's behavior. Third, a realistic EP distribution function, including sources/sinks and redistribution by the instabilities, must be used in the computation.

Counter-propagating TAE instabilities are observed on the NSTX-U device during tangential, off-axis NB injection in the co-current direction. With density of EPs from off-axis NBI peaking around mid-radius, the hollow profile developing in some discharges near the magnetic axis favors the destabilization of counter-TAEs [7]. However, detailed analysis with a realistic EP distribution shows that the positive EP density gradient near the axis is not enough to explain the positive growth rate of counter TAEs. For instance, no counter TAEs were observed in off-axis NBI experiments on the DIII-D device, in spite of the indications of hollow fast ion profiles [6]. One important difference between the scenarios in [6] and the work presented herein is that fast ions on NSTX-U are super-Alfvénic and therefore can access a broader set of resonances than on the DIII-D experiment.

The modes observed in NSTX-U have a broad radial structure that spans most of the minor radius, whereas much narrower structures are expected in devices such as ITER [4, 22]. Nevertheless, regions with large mode activity can still be accessible to EPs whose orbit width is a significant fraction of the minor radius, especially during the initial ITER operation at reduced plasma current and magnetic field. All these elements indicate that quantitative predictions of TAE stability and saturation should be performed in terms of phase space variables (E, P_ζ, μ) rather than simply assuming a predominant role of the universal TAE drive associated with the radial EP density gradient.

TRANSP analysis, augmented by a recent phase space resolved reduced EP transport model, can recover most of the experimental observations from NSTX-U. Results indicate the complex interplay between E and P_ζ gradients in driving TAEs (and possibly other Alfvénic modes) unstable. A phase space resolved analysis provides the basic indications to mitigate or suppress the observed instabilities, e.g. by populating stabilizing regions of phase space by tailored NBI. An example is shown in figure 12, in which the original discharge settings are modified in TRANSP by adding short pulses (duration 5 ms) of NB power from a more perpendicular source (identified as NB1A, with the original source named NB2A). The predicted response of the co- and counter-propagating modes studied in the previous sections is quantified through their linear growth rate and radial profile of power exchanged between modes and fast ions. For the co-propagating TAE, each pulse from the additional source results in an increase of the linear growth rate. The perpendicular NB source has a deposition profile peaked at the magnetic axis, thus increasing the radial fast ion pressure gradient, hence the growth rate of the mode. The effect is opposite for the counter-propagating TAE, for which the central deposition has stabilizing effects although the overall fast ion pressure profile remains hollow. The benefit for the actual experiment would thus be to suppress the counter-TAEs while introducing only a small perturbation to the initial NBI settings.

Overall, the results presented in this work point to the need of phase space resolved analysis for quantitative predictions of TAE stability in future scenarios (e.g. in ITER), especially when a complex EP distribution function can originate from the synergy between NBI, rf injection and alpha particles from fusion reactions.

Acknowledgments

The contribution of the NSTX-U Team is gratefully acknowledged, as well as the invaluable advice of Drs. N.N. Gorelenkov, R.B. White and G.J. Kramer (PPPL) in using the NOVA/NOVA-K and ORBIT codes. This work is supported by the U.S. Department of Energy, Office of Science, Office of Fusion Energy Sciences under contract number DE-AC02-09CH11466. NSTX-U at PPPL is a DOE Office of Science User Facility. The digital data for this paper can be found following the links from http://arks.princeton.edu/ark:/88435/dsp018p58pg29j

Notice

ORCID iDs

M. Podestà https://orcid.org/0000-0003-4975-0585

References

[1] Fasoli A. *et al* 2007 Progress in the ITER Physics Basis Chapter 5: Physics of energetic ions *Nucl. Fusion* **47** S264
[2] Heidbrink W.W. 2008 *Phys. Plasmas* **15** 055501
[3] Sharapov S. *et al* 2013 *Nucl. Fusion* **53** 104022
[4] Gorelenkov N. *et al* 2014 *Nucl. Fusion* **54** 125001
[5] McClements K.G. *et al* 2017 *Plasma Phys. Control. Fusion* **59** 053001
[6] Heidbrink W.W. *et al* 2013 *Nucl. Fusion* **53** 093006
[7] Wong H.V. *et al* 1999 *Phys. Lett.* A **251** 126
[8] Fredrickson E.D. *et al* 2000 *Phys. Plasmas* **7** 4121
[9] Menard J.E. *et al* 2012 *Nucl. Fusion* **52** 083015
[10] Hawryluk R.J. 1980 An empirical approach to tokamak transport *Physics of Plasmas Close to Thermonuclear Conditions* vol 1 (Brussels) pp 19–46
[11] Goldston R.J. *et al* 1981 *J. Comput. Phys.* **43** 61
[12] Pankin A. *et al* 2004 *Comput. Phys. Commun.* **159** 157
[13] Podestà M. *et al* 2014 *Plasma Phys. Control. Fusion* **56** 055003
[14] Podestà M. *et al* 2017 *Plasma Phys. Control. Fusion* **59** 095008
[15] Cheng C.Z. 1992 *Phys. Rep.* **211** 1–51
[16] Fu G.Y. *et al* 1992 *Phys. Fluids* B **4** 3722
[17] Gorelenkov N.N. *et al* 1999 *Phys. Plasmas* **6** 2802
[18] Podestà M. *et al* 2013 *Phys. Plasmas* **20** 082502
[19] White R.B. *et al* 1984 *Phys. Fluids* **27** 2455
[20] White R.B. 2006 *The Theory of Toroidally Confined Plasmas* 2nd edn (London: Imperial College Press)
[21] Fredrickson E.D. *et al* 2007 *Phys. Plasmas* **14** 102510
[22] Pinches S.D. *et al* 2015 *Phys. Plasmas* **22** 021807